nature materials

ARTICLES

PUBLISHED ONLINE: 18 JULY 2010 | DOI: 10.1038/NMAT2799

A multiferroic material to search for the permanent electric dipole moment of the electron

K. Z. Rushchanskii[1], S. Kamba[2], V. Goian[2], P. Vaněk[2], M. Savinov[2], J. Prokleška[3], D. Nuzhnyy[2], K. Knížek[2], F. Laufek[4], S. Eckel[5], S. K. Lamoreaux[5], A. O. Sushkov[5], M. Ležaić[1] and N. A. Spaldin[6]*

We describe the first-principles design and subsequent synthesis of a new material with the specific functionalities required for a solid-state-based search for the permanent electric dipole moment of the electron. We show computationally that perovskite-structure europium barium titanate should exhibit the required large and pressure-dependent ferroelectric polarization, local magnetic moments and absence of magnetic ordering at liquid-helium temperature. Subsequent synthesis and characterization of $Eu_{0.5}Ba_{0.5}TiO_3$ ceramics confirm the predicted desirable properties.

The standard model of particle physics incorporates the breaking of the discrete symmetries of parity (P) and the combined charge conjugation and parity (CP). It is thought, however, that the CP violation within the framework of the standard model is insufficient to explain the observed matter–antimatter asymmetry of the Universe[1]; therefore, a so-far unknown source of CP violation probably exists in nature. The existence of a non-zero permanent electric dipole moment (EDM) of a particle, such as an electron, neutron or atom, would violate time reversal (T) symmetry (Fig. 1) and therefore imply CP violation through the CPT theorem[2]. In the standard model these EDMs are strongly suppressed, the theoretical predictions lying many orders of magnitude below the present experimental limits. However, many theories beyond the standard model, such as supersymmetry, contain a number of CP-violating phases that lead to EDM predictions within experimental reach[3]. Searching for EDMs therefore constitutes a background-free method of probing the CP-violating physics beyond the standard model.

A number of experimental EDM searches are currently under way or are being developed—systems studied in these experiments include diatomic molecules[4,5], diamagnetic atoms[6–8], molecular ions[9], cold atoms[10], neutrons[11], liquids[12] and solids[13,14]—with one of the most promising new techniques being electric-field-correlated magnetization measurements in solids[15–17]. This technique rests on the fact that, as spin is the only intrinsic vector associated with the electron, a non-vanishing electron EDM is either parallel or antiparallel to its spin and hence its magnetic moment. As a result, when an electric field, which lifts the degeneracy between electrons with EDMs parallel and antiparallel to it, is applied to a sample, the associated imbalance of electron populations generates a magnetization (Fig. 2). The orientation of the magnetization is reversed when the electric field direction is switched; in our proposed experiment we shall monitor this change in sample magnetization using a SQUID magnetometer[18,19]. Such magnetoelectric responses in materials with permanent macroscopic magnetizations and polarizations are of great present interest in the materials science community because of their potential for enabling new devices that tune and control magnetism using electric fields[20].

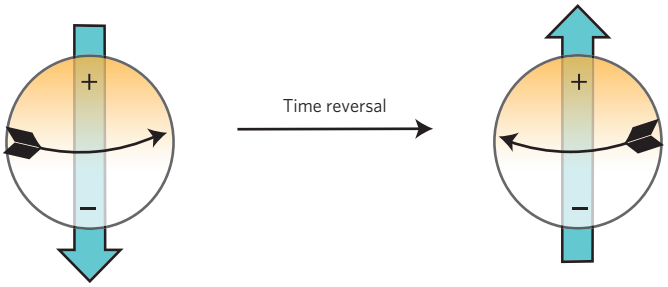

Figure 1 | Illustration that an electron with an EDM violates time-reversal symmetry. Both the EDM (+ and − symbols; orange shading) and magnetic moment (blue arrow) of the electron lie along the same axis as the electron spin (black arrow). The operation of time reversal reverses the magnetic moment but does not affect the EDM; therefore, an electron with a non-zero EDM violates time-reversal symmetry.

As the experiment aims to detect the intrinsic magnetoelectric response associated with the tiny EDM of the electron, the design constraints on the material are stringent. First, the solid must contain magnetic ions with unpaired spins, because the equal and opposite spins of paired electrons have corresponding equal and opposite EDMs and contribute no effect. These ions must be heavy, that is have large atomic number Z, as the response is roughly proportional to Z^3. Second, it must be engineered such that the conventional linear magnetoelectric tensor is zero; our approach to achieving this is to use a paramagnet in which the conventional effect is forbidden by time-reversal symmetry[21]. To reach the required sensitivity, a high atomic density of magnetic ions ($n \approx 10^{22}$ cm^{-3}) is needed, and these magnetic ions must reside at sites with broken inversion symmetry. The energy splitting Δ shown in Fig. 2 is proportional to the product of the effective electric field experienced by the electron, E^*, and its EDM, d_e. The effective electric field, which is equal to the electric field we would have

[1]Institut für Festkörperforschung, Forschungszentrum Jülich GmbH, 52425 Jülich and JARA-FIT, Germany, [2]Institute of Physics ASCR, Na Slovance 2, 182 21 Prague 8, Czech Republic, [3]Charles University, Faculty of Mathematics and Physics, Department of Condensed Matter Physics, Ke Karlovu 5, 121 16 Prague 2, Czech Republic, [4]Czech Geological Survey, Geologická 6, 152 00 Prague 5, Czech Republic, [5]Yale University, Department of Physics, PO Box 208120, New Haven, Connecticut 06520-8120, USA, [6]Materials Department, University of California, Santa Barbara, California 93106-5050, USA.
*e-mail: nicola@mrl.ucsb.edu.

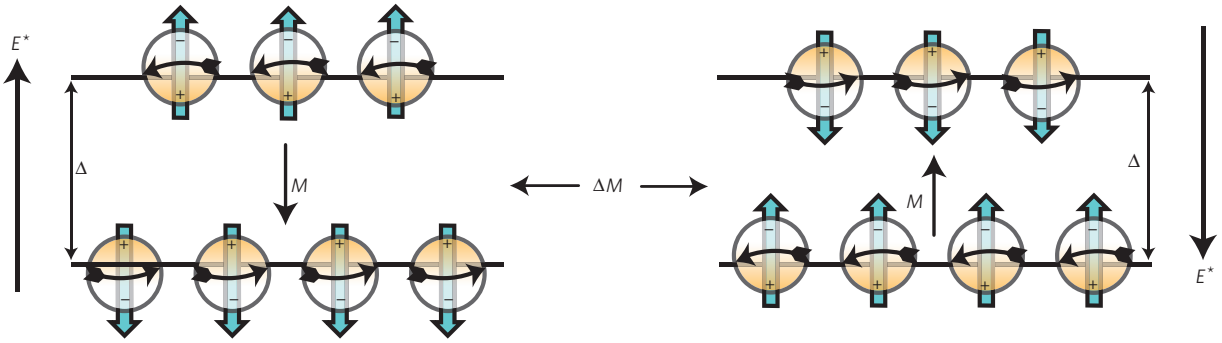

Figure 2 | Schematic of the physics underlying the experiment to search for the electron EDM. The energy of electrons with EDMs parallel to the effective electric field E^* is lower than that for electrons with anti-parallel EDMs by an amount $\Delta = E^* \cdot d_e$. As a result, there is a population imbalance (exaggerated for clarity in the figure), and, as the magnetic moments are oriented along the EDM directions, a corresponding net magnetization, M. When the electric field is reversed there is a magnetization reversal, ΔM, which can be detected using a sensitive magnetometer.

to apply to a free electron to obtain the same energy splitting, is in turn determined by the displacement of the magnetic ion from the centre of its coordination polyhedron; for a detailed derivation see ref. 22. For example, in $Eu_{0.5}Ba_{0.5}TiO_3$ ceramics (see below) with $\sim 1\,\mu C\,cm^{-2}$ remanent polarization, the mean displacement of the Eu^{2+} ion with respect to its oxygen cage is 0.01 Å and this results in an effective electric field of $\sim 10\,MV\,cm^{-1}$, even when no external electric field is applied. We choose a ferroelectric so that it is possible to reverse the direction of the ionic displacements, and hence of the effective electric field, with a moderate applied electric field. Finally, the experiment will be carried out inside liquid helium, so the materials properties described above must persist at low temperature. A detailed derivation of the dependence of the sensitivity on the materials parameters is given in ref. 19. Note that conventional impurities such as defects or domain walls are not detrimental to the experiment because they do not violate time-reversal symmetry. In summary, the following material specifications will enable a sensitive EDM search to be mounted. (1) The material should be ferroelectric, with a large electric polarization, and switchable at liquid-He temperature. (2) There should be a high concentration of heavy ions with local magnetic moments that remain paramagnetic at liquid-He temperature; both long-range order and freezing into a glassy state must be avoided. (3) The local environment at each magnetic ion should be strongly modified by the ferroelectric switching, and (4) the sample should be macroscopic. With these materials properties, and optimal SQUID noise levels, the projected experimental sensitivity is 10^{-28} e cm after ten days of averaging[19].

No known materials meet all the requirements. Indeed the contraindication between ferroelectricity and magnetism has been studied extensively over the past decade in the context of multiferroics[23], where the goal has been to achieve simultaneous ferroelectric and ferromagnetic ordering at high temperature. In spite of extensive efforts, a multiferroic with large and robust ferroelectricity and magnetization at room temperature remains elusive. Although the low-temperature constraints imposed here seem at first sight more straightforward, avoiding any magnetic ordering at low temperature, while retaining a high concentration of magnetic ions, poses a similarly demanding challenge. In addition, the problem of ferroelectric switchability at low temperature is challenging, because coercivities tend to increase as temperature is lowered[24].

We proceed by proposing a trial compound and calculating its properties using density functional theory to determine whether an experimental synthesis should be motivated. We choose an alloy of europium titanate, $EuTiO_3$, and barium titanate, $BaTiO_3$, with motivation as follows: to incorporate magnetism we require unfilled orbital manifolds of localized electrons; to avoid magnetic ordering the exchange interactions should be small. Therefore, the tightly bound 4*f* electrons are likely to be the best choice. For conventional ferroelectricity we require transition-metal ions with empty *d* orbitals to allow for good hybridization with coordinating anions on off-centring[25]. (Note that although here we use a conventional ferroelectric mechanism, many alternative routes to ferroelectricity that are compatible with magnetism—and which could form a basis for future explorations—have been recently identified; for a review see ref. 26.) Both $EuTiO_3$ and $BaTiO_3$ form in the ABO_3 perovskite structure, with divalent Eu^{2+} or Ba^{2+} on the A site, and formally d^0 Ti^{4+} on the B site. $BaTiO_3$ is a prototypical ferroelectric with a large room-temperature polarization of $25\,\mu C\,cm^{-2}$ (ref. 27). In the cubic paraelectric phase its lattice constant is 3.996 Å (ref. 28). The Ba^{2+} ion has an inert-gas electron configuration and hence zero magnetic moment.

The lattice parameter of $EuTiO_3$ is 3.905 Å (ref. 29), notably smaller than that of $BaTiO_3$. It is not ferroelectric, but has a large dielectric constant ($\epsilon \approx 400$) at low temperature, indicative of proximity to a ferroelectric phase transition; indeed, it has recently been reported to be a quantum paraelectric[29,30]. First-principles electronic-structure calculations have shown that ferroelectricity should be induced along the elongation direction by either compressive or tensile strain[31]. The Eu^{2+} ion has seven unpaired localized 4*f* electrons, resulting in a large spin magnetization of $7\,\mu_B$, and $EuTiO_3$ is an antiferromagnet with G-type ordering at a low Néel temperature of ~ 5.3 K (refs 32,33). (Independently of the study presented here, $EuTiO_3$ is of considerable present interest because its dielectric response is strongly affected by the magnetic ordering[29,30] and because of its unusual third-order magnetoelectric response[34]. These behaviours indicate coupling between the magnetic and dielectric orders caused by sensitivity of the polar soft mode to the magnetic ordering[31,35].)

Our hypothesis is that by alloying Ba on the A site of $EuTiO_3$ the magnetic ordering temperature will be suppressed through dilution, and the tendency to ferroelectricity will be increased through the expansion of the lattice constant. Our hope is to identify an alloying range in which the magnetic ordering temperature is sufficiently low while the ferroelectric polarization and the concentration of magnetic ions remain sufficiently large. In addition, we expect that the polarization will be sensitive to the lattice constant, enabling its magnitude, and consequently the coercivity, to be reduced with pressure.

First-principles calculations

Taking the 50/50 $(Eu, Ba)TiO_3$ ordered alloy as our starting point (Fig. 3 inset), we next calculate its properties using first principles. For details of the computations see the Methods section.

We began by calculating the phonon dispersion for the high-symmetry, cubic perovskite reference structure at a lattice constant

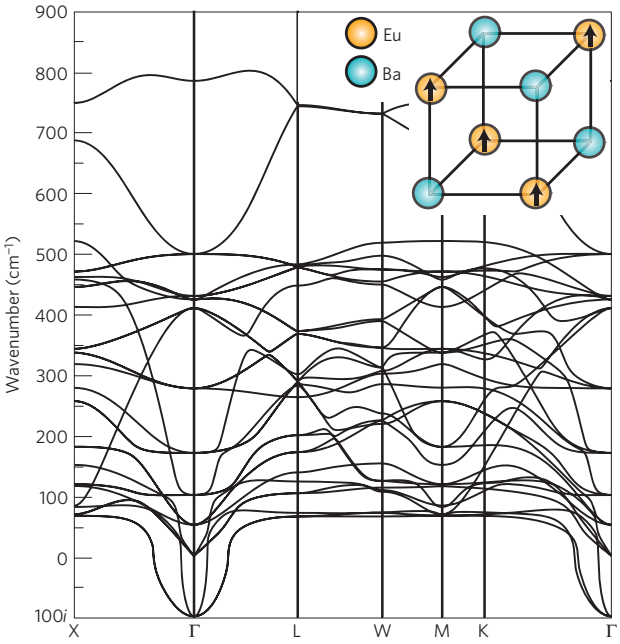

Figure 3 | Calculated phonon dispersion of ferromagnetic $Eu_{0.5}Ba_{0.5}TiO_3$ in its high-symmetry reference structure with pseudocubic lattice constant $a_0 = 3.95$ Å. The imaginary-frequency polar phonon at Γ indicates a structural instability to a ferroelectric phase. The inset shows the supercell of the ferromagnetic $Eu_{0.5}Ba_{0.5}TiO_3$ ordered alloy used in our calculations. The Ti and O ions are omitted for clarity; arrows represent the Eu magnetic moments.

of 3.95 Å (chosen, somewhat arbitrarily, for this first step because it is the average of the experimental $BaTiO_3$ and $EuTiO_3$ lattice constants), with the magnetic spins aligned ferromagnetically; our results are shown in Fig. 3, plotted along the high-symmetry lines of the Brillouin zone. Importantly, we find a polar Γ-point instability with an imaginary frequency of $103i\,cm^{-1}$, which is dominated by relative O–Ti/Eu displacements (the eigenmode displacements for Eu, Ba, Ti, $O_{\parallel}$ and $O_{\perp}$ are 0.234, −0.059, 0.394, −0.360 and −0.303 respectively); such polar instabilities are indicative of a tendency to ferroelectricity. The zone-boundary rotational instabilities that often occur in perovskite oxides and lead to non-polar, antiferrodistortive ground states are notably absent (in fact the flat bands at $\sim 60\,cm^{-1}$ are stable rotational vibrations). Interestingly, we find that the Eu ions have a significant amplitude in the soft-mode eigenvector, in contrast to the Ba ions both here and in the parent $BaTiO_3$.

Next we carried out a structural optimization of both the unit-cell shape and the ionic positions of our $Eu_{0.5}Ba_{0.5}TiO_3$ alloy with the total volume constrained to that of the ideal cubic structure studied above (3.95^3 Å^3 per formula unit). Our main finding is that the $Eu_{0.5}Ba_{0.5}TiO_3$ alloy is polar with large relative displacements of O and both Ti and Eu relative to the high-symmetry reference structure. Using the Berry phase method we obtain a ferroelectric polarization value of $P = 23\,\mu C\,cm^{-2}$. Our calculated ground state is orthorhombic with the polarization oriented along a [011] direction and lattice parameters $a = 3.94$ Å, $b = 5.60$ Å and $c = 5.59$ Å. As expected from our analysis of the soft mode, the calculated ground state is characterized by large O–Ti/Eu displacements, and the absence of rotations or tilts of the O octahedra. Importantly, the large Eu amplitude in the soft mode manifests as a large off-centring of the Eu from the centre of its O coordination polyhedron in the ground-state structure. The origin of the large Eu displacement lies in its small ionic radius compared with that of divalent Ba^{2+}. The large coordination cage around the Eu ion, which is imposed by the large lattice constant of the alloy, results in underbonding of the Eu that can be relieved by off-centring. Indeed, we find that in calculations for fully relaxed single-phase $EuTiO_3$ the oxygen octahedra tilt to reduce the volume of the A site in a similar manner to those known to occur in $SrTiO_3$, in which the A cation size is almost identical. This Eu off-centring is desirable for the EDM experiment because the change in local environment at the magnetic ions on ferroelectric switching determines the sensitivity of the EDM measurement.

Table 1 | Calculated ferroelectric polarizations, *P*, of $Eu_{0.5}Ba_{0.5}TiO_3$ at three different volumes.

Volume (Å^3)	P (μC cm^{-2})
61.63 (constrained)	23
62.30 (experimental)	28
64.63 (relaxed)	44

We note that the magnitude of the polarization is strongly dependent on the volume used in the calculation (Table 1). At the experimental volume (reported in the next section), which is only slightly larger than our constrained volume of 3.95^3 Å^3, we obtain a polarization of $28\,\mu C\,cm^{-2}$. At full relaxation, where we find a larger volume close to that of $BaTiO_3$, we obtain a polarization of $44\,\mu C\,cm^{-2}$, almost certainly a substantial overestimate. This volume dependence suggests that the use of pressure to reduce the lattice parameters and suppress the ferroelectric polarization could be a viable tool for reducing the coercivity at low temperatures. Indeed our computations show that, at a pressure corresponding to 2.8 GPa applied to the experimental volume, the theoretical structure is cubic, with both the polarization and coercive field reduced to zero.

Finally, to investigate the likelihood of magnetic ordering, we calculated the relative energies of the ferromagnetic state discussed above and of two antiferromagnetic arrangements: planes of ferromagnetically ordered spins coupled antiferromagnetically along either the pseudocubic z axis or the x or y axes. (Note that these are degenerate in the high-symmetry cubic structure.) For each magnetic arrangement we re-relaxed the lattice parameters and atomic positions. As expected for the highly localized Eu 4f electrons on their diluted sublattice, the energy differences between the different configurations are small—around 1 meV per 40-atom supercell, suggesting an absence of magnetic ordering down to low temperatures. Although our calculations find the ferromagnetic state to have the lowest energy, this is probably a consequence of our A-site ordering and should not lead us to anticipate ferromagnetism at low temperature. (Note that, after completing our study, we found a report of an early effort to synthesize (Eu, Ba)TiO_3 (ref. 36) in which a large magnetization, attributed to A-site ordering and ferromagnetism, was reported. A-site ordering is now known to be difficult to achieve in perovskite-structure oxides, however, and we find no evidence of it in our samples. Moreover, the earlier work determined a tetragonal crystal structure, in contrast to our refined orthorhombic structure.)

In summary, our predicted properties of the (Eu, Ba)TiO_3 alloy—large ferroelectric polarization, reducible with pressure, with large Eu displacements, and strongly suppressed magnetic ordering—meet the criteria for the electron EDM search and motivate the synthesis and characterization of the compound, described next.

Synthesis

$Eu_{0.5}Ba_{0.5}TiO_3$ was synthesized by solid-state reaction using mechanochemical activation before calcination. For details see the Methods section. The density of the sintered pellets was 86–88%

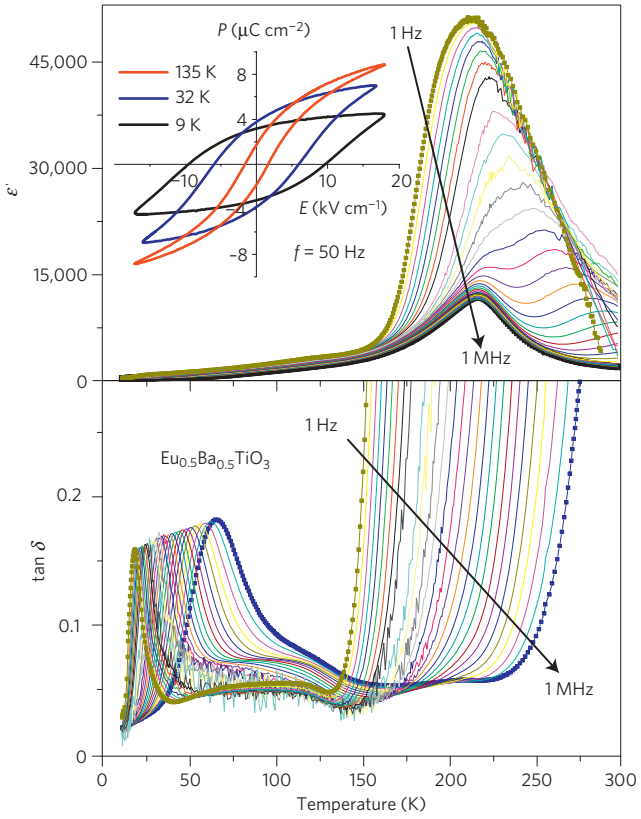

Figure 4 | Temperature dependence of permittivity and dielectric loss in $Eu_{0.5}Ba_{0.5}TiO_3$ ceramics. The arrows indicate the direction of increasing frequency and the colours are for clarity to assist the eye in distinguishing the lines. The inset shows ferroelectric hysteresis loops measured at three temperatures and 50 Hz.

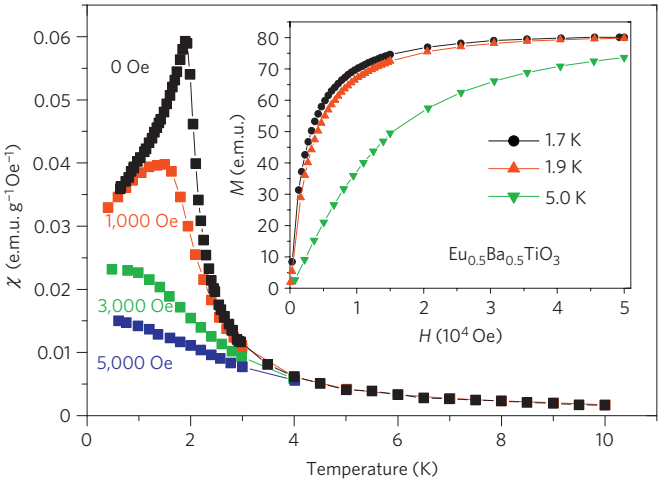

Figure 5 | Temperature dependence of ac magnetic susceptibility, χ, at various static magnetic fields and a frequency of 214 Hz. The inset shows magnetization curves at various temperatures. We note that no hysteresis in magnetization was observed.

of the theoretical density. X-ray diffraction at room temperature revealed the cubic perovskite $Pm\bar{3}m$ structure with $a = 3.9642(1)$ Å. At 100 K we obtain an orthorhombic ground state with space group $Amm2$, in agreement with our theoretical prediction, and lattice parameters 3.9563(1), 5.6069(2) and 5.5998(2) Å.

Characterization

The final step in our study is the characterization of the samples, to check that the measured properties are indeed the same as those that we predicted and desired. Figure 4 shows the temperature dependence of the complex permittivity between 1 Hz and 1 MHz, measured using an ALPHA-AN impedance analyser (Novocontrol). The low-frequency data below 100 kHz are affected above 150 K by a small defect-induced conductivity and related Maxwell–Wagner polarization; the high-frequency data clearly show a maximum in the permittivity near $T_c = 213$ K, indicating the ferroelectric phase transition. Two regions of dielectric dispersion—near 100 K and below 75 K—are seen in tan $\delta(T)$; these could originate from oxygen defects or from ferroelectric-domain-wall motion.

Measurement of the polarization was adversely affected by the sample conductivity above 150 K, but at lower temperatures good-quality ferroelectric hysteresis loops were obtained (Fig. 4, inset). At 135 K we obtain a saturation polarization of $\sim 8\,\mu C\,cm^{-2}$. The deviation from the predicted value could be the result of incomplete saturation as well as the strong volume dependence of the polarization combined with the well-known inaccuracies in GGA + U volumes. As expected, at lower temperatures the coercive field strongly increased, and only partial polarization switching was possible even with an applied electric field of $18\,kV\,cm^{-1}$ (at higher electric-field dielectric breakdown was imminent). The partial switching is responsible for the apparent decrease in saturation polarization below 40 K.

Time-domain terahertz transmission and infrared reflectivity spectra (not shown here) reveal a softening of the polar phonon from $\sim 40\,cm^{-1}$ at 300 K to $\sim 15\,cm^{-1}$ at T_c, and then its splitting into two components in the ferroelectric phase. Both components harden on cooling below T_c, with the lower-frequency component remaining near $20\,cm^{-1}$ down to 10 K and the higher-frequency branch saturating near $90\,cm^{-1}$ at 10 K. This behaviour is reminiscent of the soft-mode behaviour in $BaTiO_3$ (ref. 37). However, when we extract the contribution to the static permittivity that comes from the polar phonon, we find that it is considerably smaller than our measured value (Fig. 4), indicating an additional contribution to the dielectric relaxation. Our observations suggest that the phase transition is primarily soft-mode driven, but also exhibits some order–disorder character.

Finally, we measured the magnetic susceptibility χ at various static magnetic fields as a function of temperature T down to 0.4 K. (For details see the Methods section.) Our results are shown in Fig. 5. $\chi(T)$ peaks at $T \sim 1.9$ K, indicating an absence of magnetic ordering above this temperature. The $\chi(T)$ data up to 300 K show Curie–Weiss behaviour $\chi(T) = C/(T+\theta)$, with $\theta = -1.63$ K and $C = 0.017$ e.m.u. K g^{-1} Oe^{-1}. The peak in susceptibility at 1.9 K is frequency independent and not influenced by zero-field heating measurements after field cooling, confirming antiferromagnetic order below $T_N = 1.9$ K. As in pure $EuTiO_3$, the $\chi(T)$ peak is suppressed by a static external magnetic field, indicating stabilization of the paramagnetic phase[29]. Magnetization curves (Fig. 5 inset) show saturation above 2×10^4 Oe at temperatures below T_N and slower saturation at 5 K. No open magnetic hysteresis loops were observed.

In summary, we have designed a new material—$Eu_{0.5}Ba_{0.5}TiO_3$—with the properties required to enable a measurement of the EDM to a higher accuracy than can be realized at present. Subsequent synthesis of $Eu_{0.5}Ba_{0.5}TiO_3$ ceramics confirmed their desirable ferroelectric polarization and absence of magnetic ordering above 1.9 K. The search for the permanent dipole moment of the electron using $Eu_{0.5}Ba_{0.5}TiO_3$ is now underway. Initial measurements have already achieved an EDM upper limit of 5×10^{-23} e cm, which is within a factor of 10 of the current record with a solid-state-based EDM search[13]. We are at present studying a number of systematic effects that may mask the EDM signal. The primary error originates from ferroelectric hysteresis-induced heating of the samples during polarization reversal. This heating gives rise to a change in magnetic

susceptibility, which, in a non-zero external magnetic field, leads to an undesirable sample magnetization response. We are working to control the absolute magnetic field at the location of the samples to the 0.1 μG level. Our projected sensitivity of 10^{-28} e cm should then be achievable.

Methods

Computational details. We carried out first-principles density-functional calculations within the spin-polarized generalized gradient approximation (GGA; ref. 38). The strong on-site correlations of the Eu 4*f* electrons were treated using the GGA + *U* method[39] with the double counting treated within the Dudarev approach[40] and parameters $U = 5.7$ eV and $J = 1.0$ eV. For structural relaxation and lattice dynamics we used the Vienna *ab initio* simulation package (VASP; ref. 41) with the default projector augmented-wave (PAW) potentials[42] (valence-electron configurations: Eu, $5s^2 5p^6 4f^7 6s^2$; Ba, $5s^2 5p^6 6s^2$; Ti, $3s^2 3p^6 3d^2 4s^2$; O, $2s^2 2p^4$). Spin–orbit interaction was not included.

The 50/50 (Eu, Ba)TiO_3 alloy was represented by an ordered A-site structure with the Eu and Ba ions alternating in a checkerboard pattern (Fig. 3, inset). Structural relaxations and total-energy calculations were carried out for a 40-atom supercell (consisting of two five-atom perovskite unit cells in each Cartesian direction) using a $4 \times 4 \times 4$ Γ-centred *k*-point mesh and a plane-wave cutoff of 500 eV. Ferroelectric polarizations and Born effective charges were calculated using the Berry phase method[43]. Lattice instabilities were investigated in the frozen-phonon scheme[44,45] for an 80-atom supercell using a Γ-centred $2 \times 2 \times 2$ *k*-point mesh and 0.0056 Å atomic displacements to extract the Hellman–Feynman forces.

Synthesis. Eu_2O_3, TiO_2 (anatase) and $BaTiO_3$ powders (all from Sigma-Aldrich) were mixed in stoichiometric ratio then milled intensively in a Fritsch Pulverisette 7 planetary ball micromill for 120 min in a dry environment followed by 20 min in suspension with *n*-heptane. ZrO_2 grinding bowls (25 ml) and balls (12 mm diameter, acceleration 14 g) were used. The suspension was dried under an infrared lamp and the dried powder was pressed in a uniaxial press (330 MPa, 3 min) into 13-mm-diameter pellets. The pellets were calcined in pure H_2 atmosphere at 1,200 °C for 24 h (to reduce Eu^{3+} to Eu^{2+}), then milled and pressed by the same procedure as above and sintered at 1,300 °C for 24 h in Ar + 10% H_2 atmosphere. Note that pure H_2 cannot be used for sintering without adversely increasing the conductivity of the sample.

Characterization. Magnetic susceptibility was measured using a Quantum Design PPMS9 and a He^3 insert equipped with a home-made induction coil that enables measurement of ac magnetic susceptibility, χ, from 0.1 to 214 Hz.

Received 15 March 2010; accepted 5 June 2010; published online 18 July 2010

References

1. Trodden, M. Electroweak baryogenesis. *Rev. Mod. Phys.* **71,** 1463–1500 (1999).
2. Khriplovich, I. B. & Lamoreaux, S. K. *CP Violation Without Strangeness* (Springer, 1997).
3. Bernreuther, W. & Suzuki, M. The electric dipole moment of the electron. *Rev. Mod. Phys.* **63,** 313–340 (1991).
4. Hudson, J. J., Sauer, B. E., Tarbutt, M. R. & Hinds, E. A. Measurement of the electron electric dipole moment using YbF molecules. *Phys. Rev. Lett.* **89,** 023003 (2002).
5. Kawall, D., Bay, F., Bickman, S., Jiang, Y. & DeMille, D. Precision Zeeman–Stark spectroscopy of the metastable a(1)[$^3\sigma^+$] state of PbO. *Phys. Rev. Lett.* **92,** 133007 (2004).
6. Griffith, W. C. *et al.* Improved limit on the permanent electric dipole moment of ^{199}Hg. *Phys. Rev. Lett.* **102,** 101601 (2009).
7. Guest, J. R. *et al.* Laser trapping of ^{225}Ra and ^{226}Ra with repumping by room-temperature blackbody radiation. *Phys. Rev. Lett.* **98,** 093001 (2007).
8. Tardiff, E. R. *et al.* Polarization and relaxation of ^{209}Rn. *Nucl. Instrum. Methods Phys. Res. A* **579,** 472–475 (2007).
9. Stutz, R. P. & Cornell, E. A. Search for the electron EDM using trapped molecular ions. *Bull. Am. Phys. Soc.* DAMOP04, J1.047 (2004).
10. Weiss, D. S., Fang, F. & Chen, J. Measuring the electric dipole moment of Cs and Rb in an optical lattice. *Bull. Am. Phys. Soc.* APR03, J1.008 (2003).
11. Baker, C. A. *et al.* Improved experimental limit on the electric dipole moment of the neutron. *Phys. Rev. Lett.* **97,** 131801 (2006).
12. Ledbetter, M. P., Savukov, I. M. & Romalis, M. V. Nonlinear amplification of small spin precession using long-range dipolar interactions. *Phys. Rev. Lett.* **94,** 060801 (2005).
13. Heidenreich, B. J. *et al.* Limit on the electron electric dipole moment in gadolinium–iron garnet. *Phys. Rev. Lett.* **95,** 253004 (2005).
14. Bouchard, L. S., Sushkov, A. O., Budker, D., Ford, J. J. & Lipton, A. S. Nuclear-spin relaxation of ^{207}Pb in ferroelectric powders. *Phys. Rev. A* **77,** 022102 (2008).
15. Shapiro, F. L. Electric dipole moments of elementary particles. *Sov. Phys. Usp.* **11,** 345–352 (1968).
16. Lamoreaux, S. K. Solid-state systems for the electron electric dipole moment and other fundamental measurements. *Phys. Rev. A* **66,** 022109 (2002).
17. Budker, D., Lamoreaux, S. K., Sushkov, A. O. & Sushkov, O. P. Sensitivity of condensed-matter P- and T-violation experiments. *Phys. Rev. A* **73,** 022107 (2006).
18. Sushkov, A. O., Eckel, S. & Lamoreaux, S. K. Prospects for a new search for the electron electric-dipole moment in solid gadolinium–iron-garnet ceramics. *Phys. Rev. A* **79,** 022118–8 (2009).
19. Sushkov, A. O., Eckel, S. & Lamoreaux, S. K. The prospects for an electron electric dipole moment search with ferroelectric (Eu, Ba)TiO_3 ceramics. *Phys. Rev. A* **81,** 022104 (2010).
20. Spaldin, N. A. & Ramesh, R. Electric-field control of magnetism in complex oxide thin films. *MRS Bull.* **33,** 1047–1050 (2008).
21. Fiebig, M. Revival of the magnetoelectric effect. *J. Phys. D* **38,** R1–R30 (2005).
22. Mukhamedjanov, T. N., Dzuba, V. A. & Sushkov, O. P. Enhancement of the electron electric dipole moment in gadolinium garnets. *Phys. Rev. A* **68,** 042103 (2003).
23. Hill, N. A. Why are there so few magnetic ferroelectrics? *J. Phys. Chem. B* **104,** 6694–6709 (2000).
24. Merz, W. J. The dielectric properties of $BaTiO_3$ at low temperatures. *Phys. Rev.* **81,** 1064–1065 (1951).
25. Rondinelli, J. M., Eidelson, A. S. & Spaldin, N. A. Non-d^0 Mn-driven ferroelectricity in antiferromagnetic $BaMnO_3$. *Phys. Rev. B* **79,** 205119 (2009).
26. Ramesh, R. & Spaldin, N. A. Multiferroics: Progress and prospects in thin films. *Nature Mater.* **6,** 21–29 (2007).
27. Wemple, S. Jr & Camlibel, M. D. Dielectric and optical properties of melt-grown $BaTiO_3$. *J. Phys. Chem. Solids* **29,** 1797–1803 (1968).
28. Miyake, S. & Ueda, R. On phase transformation of $BaTiO_3$. *J. Phys. Soc. Jpn* **2,** 93–97 (1947).
29. Katsufuji, T. & Takagi, H. Coupling between magnetism and dielectric properties in quantum paraelectric $EuTiO_3$. *Phys. Rev. B* **64,** 054415 (2001).
30. Kamba, S. *et al.* Magnetodielectric effect and optic soft mode behaviour in quantum paraelectric $EuTiO_3$ ceramics. *Europhys. Lett.* **80,** 27002 (2007).
31. Fennie, C. J. & Rabe, K. M. Magnetic and electric phase control in epitaxial $EuTiO_3$ from first principles. *Phys. Rev. Lett.* **97,** 267602 (2006).
32. McGuire, T. R., Shafer, M. W., Joenk, R. J., Alperin, H. A. & Pickart, S. J. Magnetic structure of $EuTiO_3$. *J. Appl. Phys.* **37,** 981–982 (1966).
33. Chien, C-L., DeBenedetti, S. & Barros, F. D. S. Magnetic properties of $EuTiO_3$, Eu_2TiO_4, and $Eu_3Ti_2O_7$. *Phys. Rev. B* **10,** 3913–3922 (1974).
34. Shvartsman, V. V., Borisov, P., Kleemann, W., Kamba, S. & Katsufuji, T. Large off-diagonal magnetoelectric coupling in the quantum paraelectric antiferromagnet $EuTiO_3$. *Phys. Rev. B* **81,** 064426 (2010).
35. Goian, V. *et al.* Polar phonon mixing in magnetoelectric $EuTiO_3$. *Eur. Phys. J. B* **71,** 429–433 (2009).
36. Janes, D. L., Bodnar, R. E. & Taylor, A. L. Europium barium titanate—a magnetic ferroelectric compound. *J. Appl. Phys.* **49,** 1452–1454 (1978).
37. Hlinka, J. *et al.* Coexistence of the phonon and relaxation soft mode in the terahertz dielectric response of tetragonal $BaTiO_3$. *Phys. Rev. Lett.* **101,** 167402 (2008).
38. Perdew, J. P., Burke, K. & Ernzerhof, M. Generalized gradient approximation made simple. *Phys. Rev. Lett.* **77,** 3865–3868 (1996).
39. Anisimov, V. I., Aryasetiawan, F. & Liechtenstein, A. I. First-principles calculations of the electronic structure and spectra of strongly correlated systems: The LDA+U method. *J. Phys. Condens. Matter* **9,** 767–808 (1997).
40. Dudarev, S. L., Botton, G. A., Savrasov, S. Y., Humphreys, C. J. & Sutton, A. P. Electron-energy-loss spectra and the structural stability of nickel oxide: An LSDA+U study. *Phys. Rev. B* **57,** 1505–1509 (1998).
41. Kresse, G. & Furthmüller, J. Efficient iterative schemes for *ab initio* total-energy calculations using a plane-wave basis set. *Phys. Rev. B* **54,** 11169–11186 (1996).
42. Blöchl, P. E. Projector augmented-wave method. *Phys. Rev. B* **50,** 17953–17979 (1994).
43. King-Smith, R. D. & Vanderbilt, D. Theory of polarization of crystalline solids. *Phys. Rev. B* **47,** 1651–1654 (1993).
44. Kunc, K. & Martin, R. M. *Ab initio* force constants of GaAs: A new approach to calculation of phonons and dielectric properties. *Phys. Rev. Lett.* **48,** 406–409 (1982).
45. Alfe, D. PHON: A program to calculate phonons using the small displacement method. *Comp. Phys. Comm.* **180,** 2622–2633 (2009).

Acknowledgements

This work was supported by the US National Science Foundation under award number DMR-0940420 (NAS), by Yale University, by the Czech Science Foundation (project Nos. 202/09/0682 and AVOZ10100520) and by the Young Investigators Group Programme of the Helmholtz Association, Germany, contract VH-NG-409. We thank O. Pacherova, R. Krupkova and G. Urbanova for technical assistance and O. Sushkov for discussions.

Author contributions

S.K.L. supervised the EDM measurement effort at Yale. A.O.S. and S.E. carried out the analysis and made preliminary measurements, showing that these materials could be useful in an EDM experiment. M.L. and N.A.S. selected $(Eu, Ba)TiO_3$ as the candidate material according to the experimental requirements and supervised the *ab initio* calculations. K.Z.R. carried out the *ab initio* calculations. M.L., N.A.S. and K.Z.R. analysed the *ab initio* results and wrote the theoretical component of the paper. Ceramics were prepared by P.V. Crystal structure was determined by K.K. and F.L. Dielectric measurements were carried out by M.S. J.P. investigated magnetic properties of ceramics. V.G. carried out infrared reflectivity studies. D.N. investigated terahertz spectra. S.K. coordinated all experimental studies and wrote the synthesis and characterization part of the manuscript. N.A.S. coordinated the preparation of the manuscript.

Additional information

The authors declare no competing financial interests. Reprints and permissions information is available online at http://npg.nature.com/reprintsandpermissions. Correspondence and requests for materials should be addressed to N.A.S.